*International Journal of Innovative Computing, Information and Control*
Volume **5**, Number **0x**, x **2009**
ICIC International ©2010 ISSN 1349-4198
pp. **0–0**

# BIFURCATION ANALYSIS OF NOISE-INDUCED SYNCHRONIZATION

Katsutoshi Yoshida

Department of Mechanical Systems Engineering
Utsunomiya University
7-1-2 Yoto, Utsunomiya-shi, Tochigi 321-8585, Japan
yoshidak@cc.utsunomiya-u.ac.jp

Yusuke Nishizawa

ShinMaywa Industries, Ltd.
1-1 Shinmeiwa-cho, Takarazuka-shi, Hyogo 665-8550, Japan

Abstract. We investigate bifurcation phenomena between slow and fast convergences of synchronization errors arising in the proposed synchronization system consisting of two identical nonlinear dynamical systems linked by a common noisy input only. The numerical continuation of the saddle-node bifurcation set of the primary resonance of moments provides an effective identifier of the slow convergence of synchronization errors.

**Keywords:** Noise, Synchronization, Bifurcation, Statistical Equivalent Approach.

1. **Introduction.** The noise-induced synchronization of a dynamical system with its copies can easily be found in nonlinear systems, such as the discrete maps[1, 2], the Lorenz system[1], the Duffing oscillator[3], the single mode $CO_2$ laser[4], and the uncoupled neurons[5]. One of the most important results of them is that the perfect synchronization may arise under some suitable conditions[1, 3, 4]. Moreover, the perfect synchronization exhibits significant degree of robustness against mismatches among the copies such as the parameters mismatch[3] and the independent random fluctuations of the copies[1, 6]. Furthermore, regarding the response of the synchronization system as a Markov process to derive the transition law of it, we have analytically shown that the perfect synchronization can be regarded as an absorbing barrier of the Markov process[7].

In these studies, however, little research have been done on transient behavior to approach the perfect synchronization. In engineering applications, too slow convergence of synchronization errors would be regarded as failing to converge, even if the synchronization is achieved mathematically. In practice, the perfect synchronization is possibly applicable to synchronizing initial conditions of coexisting oscillators with a common specification such as independent subcircuits in a circuit system, independent mechanical vibrators on bench testing, and so on. However, it is hardly applicable to industrial purposes when the convergence speed is too slow.

To solve this problem, we have already investigated how to characterize the slow convergence of synchronization errors[8, 9], showing that the slow convergence is related to the slow diffusions caused by multimodal probability densities so that it can be detected as multi-valued solutions of the moment differential equations (MDE).

In this paper, we perform nonlinear analysis on the MDE. We first construct Poincaré maps of periodic solutions of the MDE to examine asymptotic behavior of the moments and clarify that the primary resonance encounters a saddle-node bifurcation. We then numerically continue the bifurcation point to obtain the saddle-node bifurcation set that is in good agreement with the threshold of occurrence of the slow convergence.

## 2. Noise-induced Synchronization.

**2.1. Slow convergence of synchronization errors.** Let us consider the pair of identical piecewise linear systems[8, 9]:

$$\begin{aligned} \ddot{x} + c\dot{x} + kG(x;\mu) &= Q + u(t), \\ \ddot{y} + c\dot{y} + kG(y;\mu) &= Q + u(t). \end{aligned} \tag{1}$$

where $Q$ is a preload, $u(t)$ is a random input, and the function $G$ is a piecewise linear function defined by $G(x;\mu) = (x+\mu) - |x+\mu| + (x-\mu) + |x-\mu|$ describing a linear spring with a dead zone of the width $2\mu$. In the previous work[9], we have examined the two types of the input $u(t)$ such as the combination of the harmonic forcing and white noise:

$$u(t) = P\cos(\omega t) + sw(t), \tag{2}$$

and the filtered noise:

$$\ddot{u} + 2\zeta\omega_n\dot{u} + \omega_n^2 u = sw(t), \tag{3}$$

where $w(t)$ is the standard Gaussian white noise. It is shown that the synchronization system (1) produces the perfect synchronization where the synchronization error vanishes deterministically.

On the contrary, in the present work, we consider the random-phase harmonic forcing as a purely random input in the following form:

$$u(t) = P\cos\Big(\omega t + \rho B_t\Big) \tag{4}$$

where $B_t$ is the standard Brownian motion. We choose $c = 0.04$, $k = 1.0$, $\mu = 0.7$, $Q = 0.3$, $P = 0.2$, and $\rho = 2\times 10^{-5}$ which produce both the fast and slow convergence by sweeping $\omega$ and can be implemented easily as a realistic mechanical structure.

Figure 1 shows sample paths of synchronization errors for $\omega = 0.8$ (upper side) and 0.95 (lower side) respectively. There is significant difference in convergence time between the two conditions. The convergence times are $t > 20000$ and $t = 118$ respectively. This means that one spends time to converge more than 169 times as much as the other.

**2.2. Localization of probability densities.** One explanation of the slow convergence of the synchronization errors is the transient localization of probability densities as already discussed by the authors[9].

One of the pair (1), say a single system, produces the transient probability density $p(x_1, x_2, t)$ satisfying the following Fokker-Plank-Kolmogorov (FPK) equation:

$$\frac{\partial p}{\partial t} = \frac{\rho^2}{2}\frac{\partial^2 p}{\partial x_3^2} - \frac{\partial(\omega p)}{\partial x_3} - \frac{\partial(x_2 p)}{\partial x_1} - \frac{\partial}{\partial x_2}\Big(-cx_2 - k\,G(x_1;\mu) + Q + P\cos x_3\Big)p \tag{5}$$

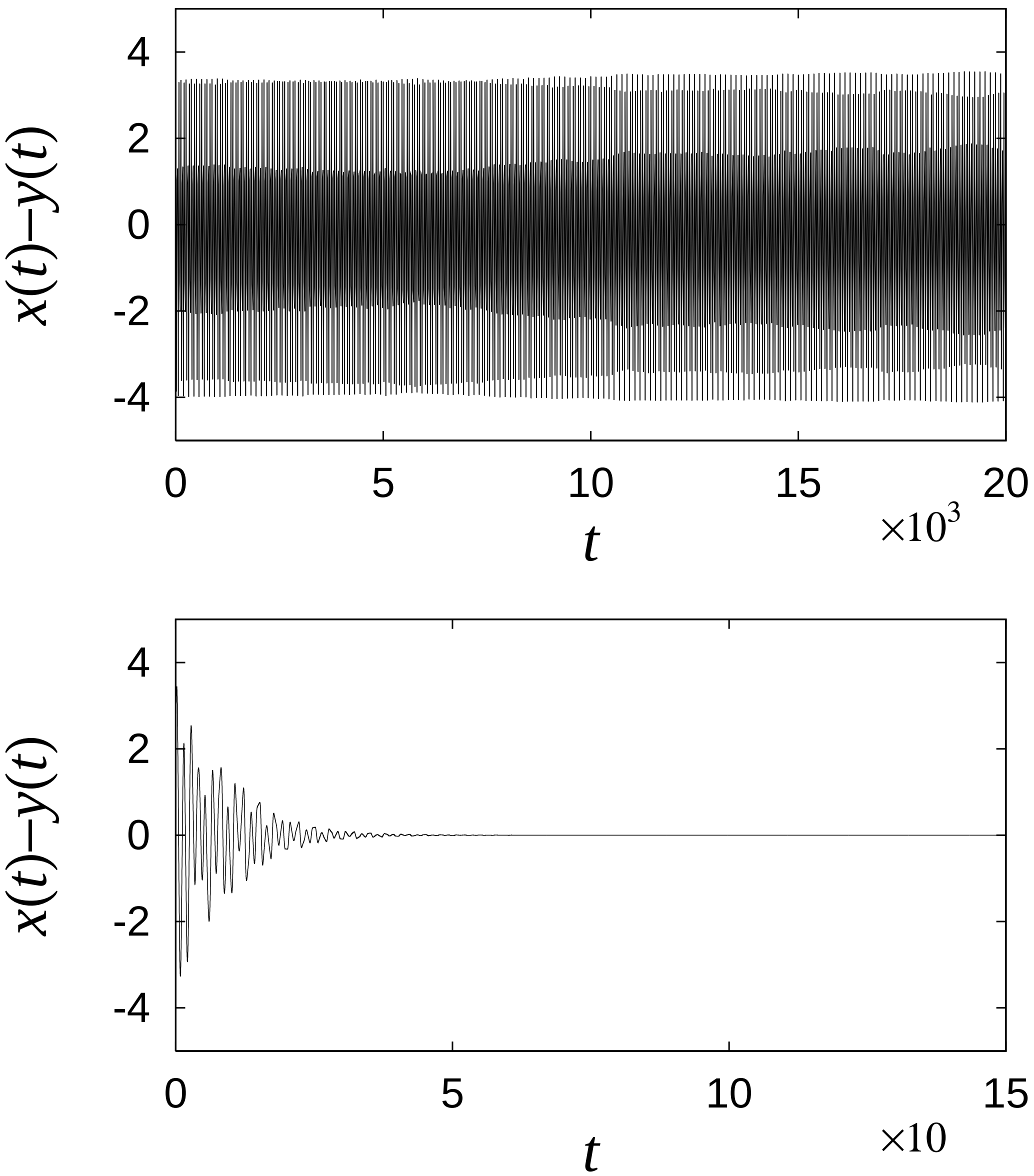


FIGURE 1. Sample paths of synchronization errors for $\omega = 0.8$ (upper) and 0.95 (lower) respectively.

where $x_1 := x$, $x_2 := \dot{x}$, $x_3 := B_t$. To obtain direct solutions of these equations, we employ Monte-Carlo techniques where the densities are obtained from cumulative frequencies over the 10000 samples of numerical solutions of one of the pair (1).

Figure 2 shows dependency of the solution $p(x_1, x_2, t)$ of the FPK equation (5) on the initial conditions $p(x_1, x_2, 0)$. The small graphs represent the probability densities at $t = 60 \times 2\pi/\omega$ starting from the initial functions $p(x_1, x_2, 0) = \delta(x_1 - 2)\delta(x_2 - 2)$ in the upper side and $\delta(x_1 + 0.5)\delta(x_2)$ in the lower side respectively. It is obviously seen that the transient densities significantly depend on the initial conditions within the region $\omega \in [0.76, 0.92]$. In case of $\omega = 0.76$, both the initial conditions (a) and (b) cause quite

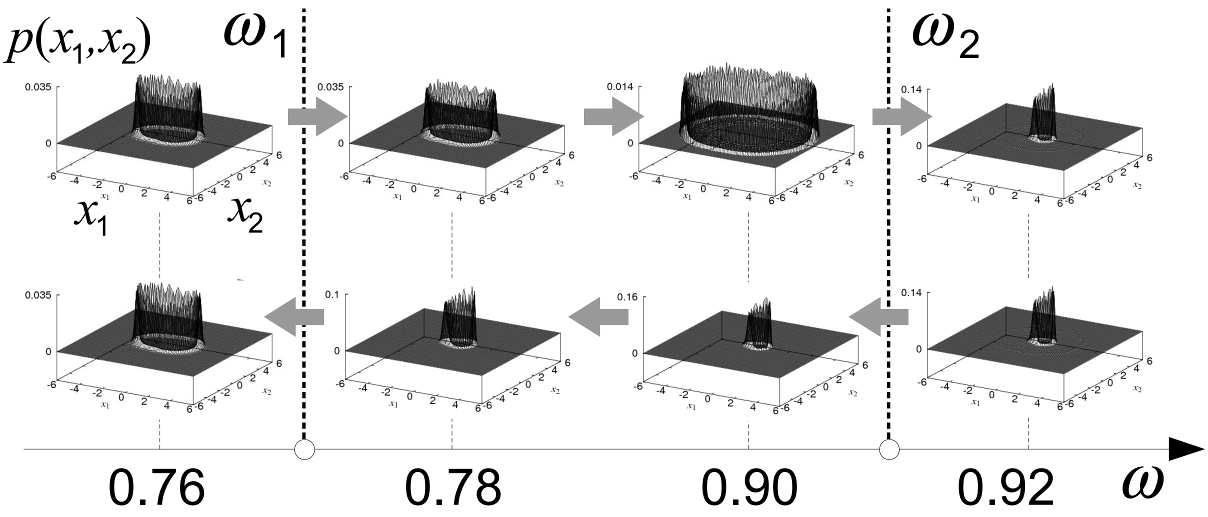


FIGURE 2. Transient isolation of probability densities at $t = 60 \times 2\pi/\omega$ comparable with deterministic hysteric jumps.

similar densities so that dependency on the initial conditions is hardly found in this case. As $\omega$ increases to 0.78, the outer ring found at $\omega = 0.76$ is being replaced with the smaller ring for (a) while the previous state maintains for (b). Further increase of $\omega$ cause second change of the densities at $\omega = 0.92$ where the outer ring of (b) at $\omega = 0.9$ is being replaced with the smaller ring of (b) at $\omega = 0.92$ while the densities of (a) maintains between $\omega = 0.9$ and 0.92.

In the previous work[9], we have already discussed that this dependency on initial conditions, in other words, the transient isolation of the densities is one of the main reasons of the slow convergence of the synchronization errors and can be detected by hysteric jumps of statistical moments. It will be shown that similar results can be obtained even in this work considering the random-phase forcing (4).

2.3. **Moment equations.** In order to evaluate the statistical moments of the synchronization, we derive the moment differential equations (MDE) from the FPK equation (5) as follows.

$$\begin{aligned}
&\dot{m_1} = m_2,\ \dot{m_2} = -cm_2 - k\langle G\rangle + Q + P\langle \cos x_3\rangle,\\
&\dot{m_3} = \omega,\ \dot{\sigma_{11}} = 2\sigma_{12},\\
&\dot{\sigma_{12}} = \sigma_{22} - c\sigma_{12} - k\langle (x_1 - m_1)G\rangle + P\langle x_1 \cos x_3\rangle,\\
&\dot{\sigma_{13}} = \sigma_{23} + \omega m_1,\\
&\dot{\sigma_{22}} = -2c\sigma_{22} - 2k\langle (x_2 - m_2)G\rangle + 2P\langle x_2 \cos x_3\rangle,\\
&\dot{\sigma_{23}} = -c\sigma_{23} - k\langle (x_3 - m_3)G\rangle + P\langle x_3 \cos x_3\rangle - \omega m_2,\\
&\dot{\sigma_{33}} = 2\omega m_3 + \rho^2
\end{aligned} \tag{6}$$

where $m_i = \langle x_i\rangle$, $\sigma_{ij} = \langle (x_i - m_i)(x_j - m_j)\rangle$. The nonlinear averages are linearized by the standard statistically equivalent techniques[10, 11]. In our case, however, $x_3 = B_t$ is hardly assumed to be Gaussian because $B_t$ is unbounded. Therefore, utilizing the formula of the Brownian motion[12]:

$$\langle f(B_t)\rangle = \frac{1}{\sqrt{2\pi t}}\int_{-\infty}^{\infty} f(x)e^{-x^2/2}dx, \tag{7}$$

we perform the approximation $\langle \cos x_3\rangle \approx e^{-\rho^2/2}\cos(m_3)$, $\langle x_3 \cos x_3\rangle \approx e^{-\rho^2/2}\sqrt{\omega m_3}\cos m_3$.

In this setup, the moment equations (6) can be regarded as a periodically forced system (reducing $\dot{m_3} = \omega$ to $m_3 = \omega t$) where the third equation of (6) is neglectable. Furthermore, in order to calculate $\sigma_{11}$ and $\sigma_{22}$ only, the sixth, eighth, and ninth equations are also neglectable because the remaining equations are not coupled with them. Therefore, we can reduce the MDE (6) into the following form:

$$\begin{aligned}
\dot{m_1} &= m_2,\\
\dot{m_2} &= -cm_2 - k\alpha_0(m_1,\sigma_{11}) + Q + Pe^{\rho^2/2}\cos\omega t,\\
\dot{\sigma_{11}} &= 2\sigma_{12},\\
\dot{\sigma_{12}} &= \sigma_{22} - c\sigma_{12} - k\alpha_1(m_1,\sigma_{11})\sigma_{11} + Pm_1e^{\rho^2/2}\cos\omega t,\\
\dot{\sigma_{22}} &= -2c\sigma_{22} - 2k\alpha_1(m_1,\sigma_{11})\sigma_{12} + 2Pm_2e^{\rho^2/2}\cos\omega t
\end{aligned} \tag{8}$$

where $\alpha_0(m_1,\sigma_{11})$ and $\alpha_1(m_1,\sigma_{11})$ are the statistically equivalent gains derived by Sato[11]:

$$\begin{aligned}
\alpha_0 &= m_1 + \sqrt{\frac{\sigma_{11}}{2\pi}}\left(e^{-\frac{(m_1-\mu)^2}{2\sigma_{11}}} + e^{-\frac{(m_1+\mu)^2}{2\sigma_{11}}}\right)\\
&+\frac{m_1+\mu}{2}\operatorname{erf}\left(-\frac{m_1+\mu}{\sqrt{2\sigma_{11}}}\right) + \frac{m_1-\mu}{2}\operatorname{erf}\left(-\frac{m_1-\mu}{\sqrt{2\sigma_{11}}}\right),
\end{aligned} \tag{9}$$

$$\alpha_1 = 1 + \frac{1}{2}\operatorname{erf}\left(-\frac{m_1+\mu}{\sqrt{2\sigma_{11}}}\right) - \frac{1}{2}\operatorname{erf}\left(-\frac{m_1-\mu}{\sqrt{2\sigma_{11}}}\right) \tag{10}$$

where $\operatorname{erf}(\cdot)$ is the error function. Therefore, in what follows, we calculate $\sigma_{11}$ and $\sigma_{22}$ from final expression (8).

2.4. **Jumps of moments.** Figure 3 shows the peak-to-peak values of $\langle x_1^2\rangle = \sigma_{22}$ calculated from the reduced MDE (8) and the mean convergence time[9]:

$$\langle T\rangle := \frac{1}{K}\sum_{k=1}^{K}\min\left\{ n \,\middle|\, \sup_{1\le i,j\le M} |X_k^i(n) - X_k^j(n)| < \epsilon \right\} \tag{11}$$

where $n$ is a discrete time s.t. $t = n\Delta t$, $\{X_k^m(n)\}_{m=1}^M$ is the $k$-th set of $M$ points composing numerical probability densities, $k$ represents the $k$-th sample path of the random excitation, and $\epsilon \ll 1$ is a criterion of the convergence. The moments are calculated as numerical solutions of the moment equations (8). The solid and broken curves indicate the forward and backward sweeps of the frequency $\omega$ respectively. The mean convergence time $\langle T\rangle$ is estimated by substituting numerical solutions of (1) starting from $5\times 5$ uniform Cartesian grids on the region $(x_1,x_2)\in[-10,10]\times[-10,10]$ into Eq.(11) where $M = 5\times 5 = 25$, $K = 100$, $\epsilon = 10^{-5}$. The plots of $\langle T\rangle$ are saturated at the given value $\langle T\rangle_{\max} = 3000$.

It is clearly seen from Fig.3 that the mean convergence time $\langle T\rangle$ rapidly increase within the hysteric jumps of the second moment of response $\langle x_1^2\rangle$. This means that the hysteric

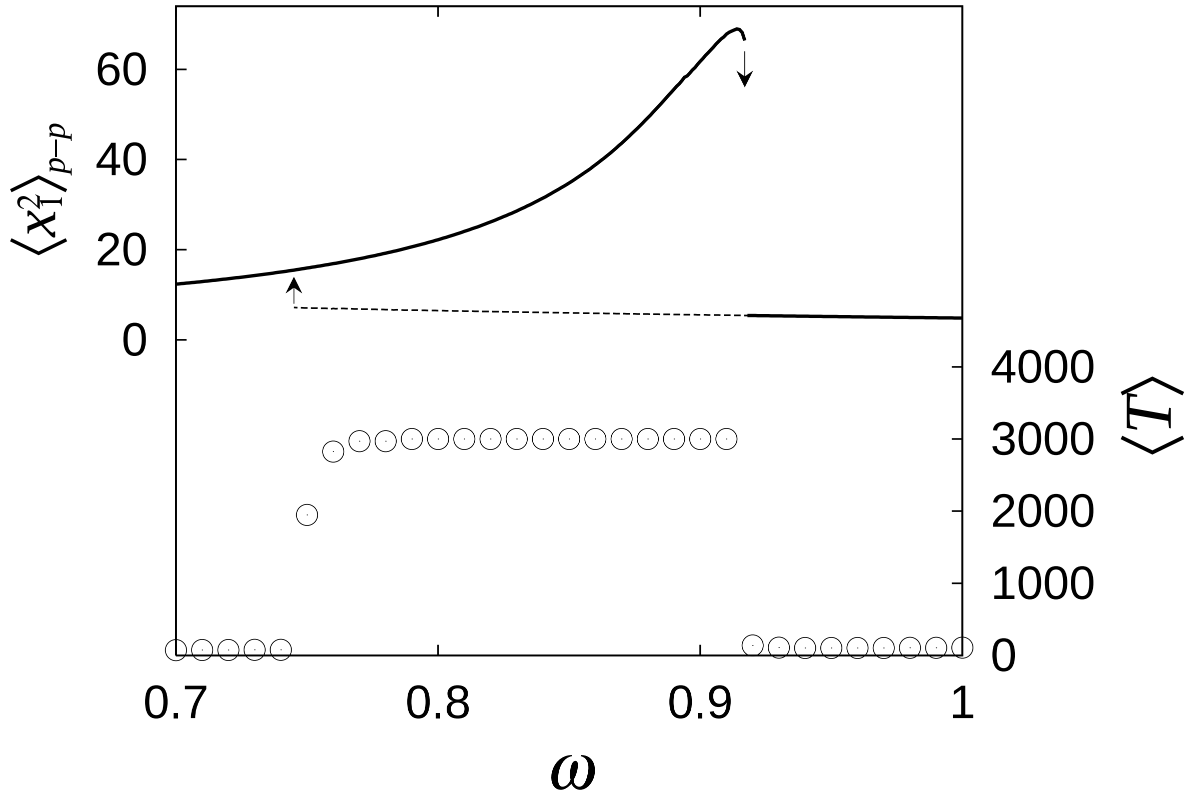


FIGURE 3. The peak-to-peak of the second moment $\langle x_1^2 \rangle_{\text{p-p}}$ and the mean convergence time $\langle T \rangle$ of the pair (1).

jumps of the moment in the statistical equivalent sense act as an identifier to indicate the slow convergence of the synchronization errors. This means that the present result based on the random phase forcing in Eq. (4) agrees with the previous result[9] considering the other types of forcing in Eqs (2) and (3).

## 3. **Bifurcation Analysis of Moments.**

3.1. **Poincaré map of moments.** Let us now rewrite the MDE (8) in the vector form:

$$\dot{\boldsymbol{q}} = \boldsymbol{f}(\boldsymbol{q}, t; p), \quad \boldsymbol{q}(0) = \boldsymbol{q}_0 \tag{12}$$

where $t \in R$ is time, $p \in R$ is a free parameter, and $\boldsymbol{q} = (m_1, m_2, \sigma_{11}, \sigma_{12}, \sigma_{22}) : R \to R^5$, $\boldsymbol{f} : R^5 \times R \to R^5$. The solution of this initial value problem can be written in the form:

$$\boldsymbol{q}(t) = \varphi(t, \boldsymbol{q}_0) \tag{13}$$

where $\varphi$ is the shift operator generated by the MDE. In our case, the function $\boldsymbol{f}$ is supposed to be periodic in time,

$$\boldsymbol{f}(\boldsymbol{q}, t + \tau; p) = \boldsymbol{f}(\boldsymbol{q}, t; p) \tag{14}$$

where $\tau = 2\pi/\omega$ is a period of the external forcing of the MDE (12). Now, we provide a brief summary of how to characterize periodic solutions of the MDE. See the reference[13]

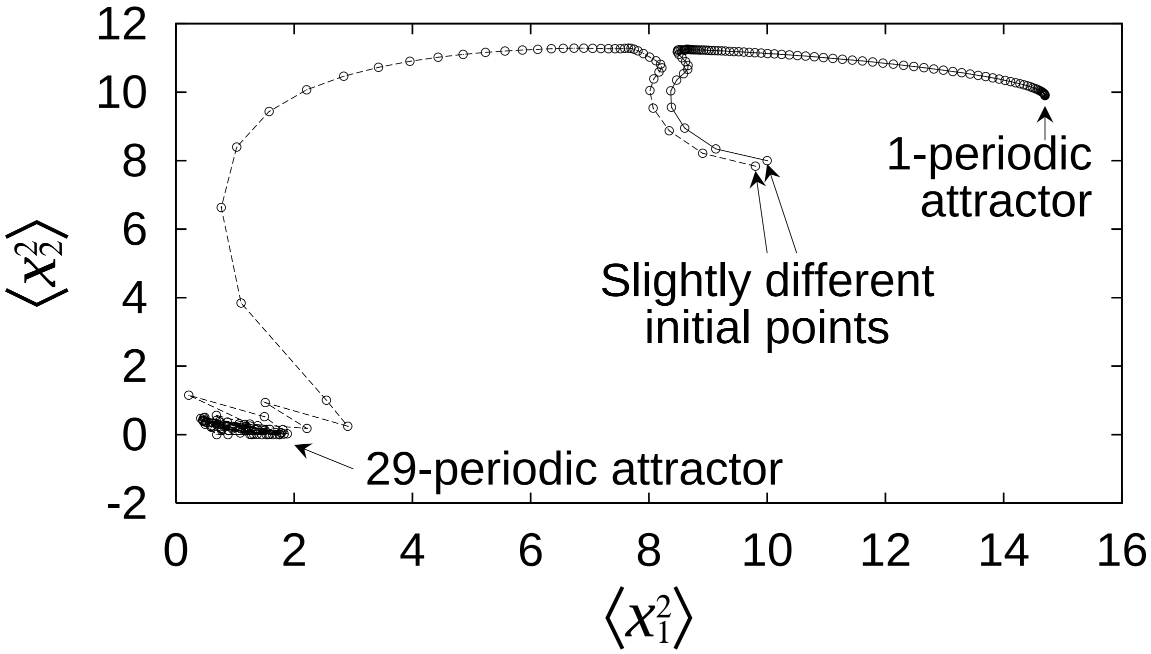


FIGURE 4. Poincaré plots of solutions of the MDE (8) for $\omega = 0.9$ starting from $\boldsymbol{q}(0) = \boldsymbol{a} = (0.5, 2.5, 10, 2, 8)$ and $0.98\boldsymbol{a}$.

for details. In order to reduce dimension, the Poincaré map is defined by,

$$T : R^5 \to R^5 : \boldsymbol{q} \mapsto \varphi(\tau, \boldsymbol{q}). \tag{15}$$

In practice, a series of points generated by the Poincaré map is obtained by $\boldsymbol{q}_k = T^k(\boldsymbol{q}_0) = \varphi(k\tau, \boldsymbol{q}_0)$ $(k = 1, 2, \cdots)$. Plotting $\boldsymbol{q}_k$ is sometimes referred to as the Poincaré plot.

Therefore, the $m$-periodic solutions passing through $\bar{\boldsymbol{q}} \in R^5$ satisfies

$$T^m(\bar{\boldsymbol{q}}) = \bar{\boldsymbol{q}}, \tag{16}$$

so that the periodic solutions can be regarded as the fixed points of the mapping $T$.

Figure 4 shows Poincaré plots of the solutions of the MDE (8) for $\omega = 0.9$, which is inside of the hysteric region of the response in Fig.3, starting from the initial points $\boldsymbol{q}(0) = \boldsymbol{a} = (0.5, 2.5, 10, 2, 8)$ and $\boldsymbol{q}(0) = 0.98\boldsymbol{a}$. It is clearly seen that the initial point $\boldsymbol{q}(0) = \boldsymbol{a}$ converges the 1-periodic attractor far from the origin while $\boldsymbol{q}(0) = 0.98\boldsymbol{a}$ converges to a 29-periodic attractor near the origin. In this case, it seems that there is a repeller near the initial points so that slight difference in initial conditions results in distinct amplitudes of response as already shown in Fig.3.

On the other hand, Fig.5 shows Poincaré plots for $\omega = 0.95$, which is outside of the hysteric region of the response in Fig.3, starting from the same initial conditions as those in Fig.4. It is obviously shown that the attractor far from the origin vanishes and the periodic attractor near the origin is replaced with a quasi-periodic attractor corresponding to a solution with infinite period. Figure 6 shows that stationary probability density of the original equation (1) under the condition corresponding to the quasi-periodic attractor in Fig.5 for $\omega = 0.95$. The two peaks of the density are caused by temporal switching orbits of the sample paths fluctuating around bistable periodic orbits of the original equation

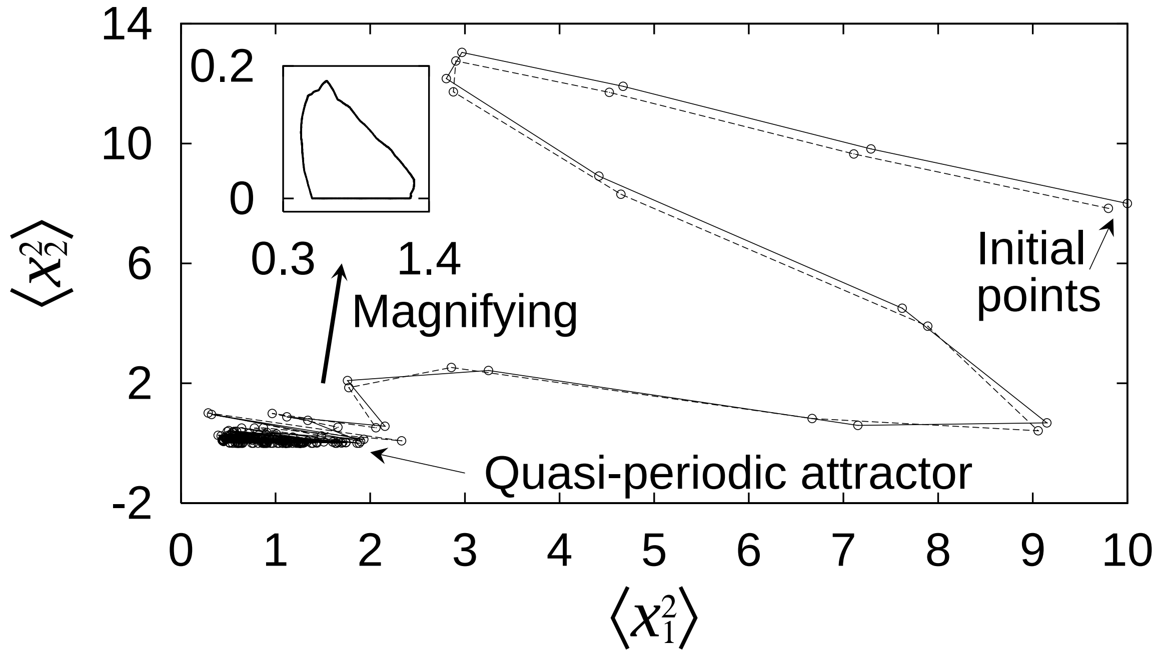


FIGURE 5. Poincaré plots of solutions of the MDE (8) for $\omega = 0.95$ starting from $\boldsymbol{q}(0) = \boldsymbol{a} = (0.5, 2.5, 10, 2, 8)$ and $0.98\boldsymbol{a}$.

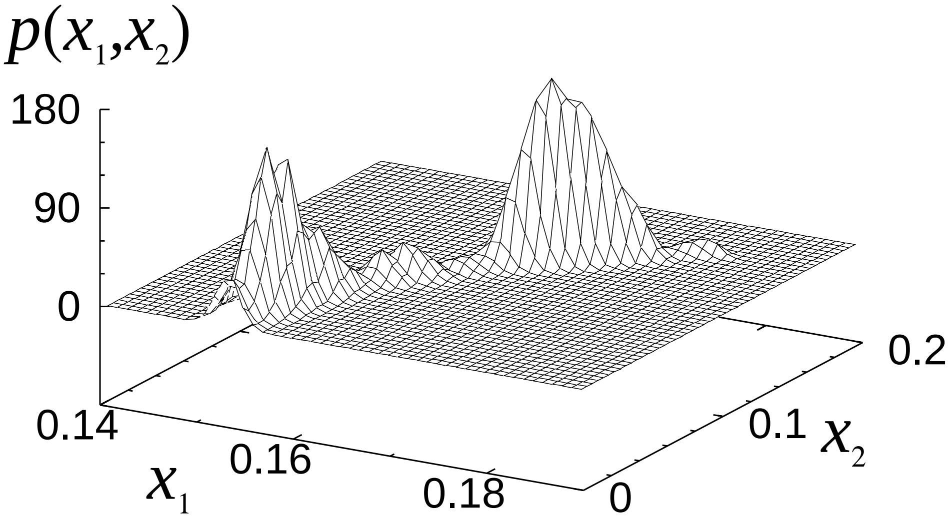


FIGURE 6. Stationary probability density of the original SDE (1) under the condition corresponding to the quasi-periodic attractor in Fig.5 for $\omega = 0.95$. Quasi-periodicity is hardly observed.

(1) under the deterministic limit. It follows that the quasi-periodicity of the MDE does not reflect this bistability of the sample paths. One explanation of this disagreement is the approximation errors of the nonlinear moments.

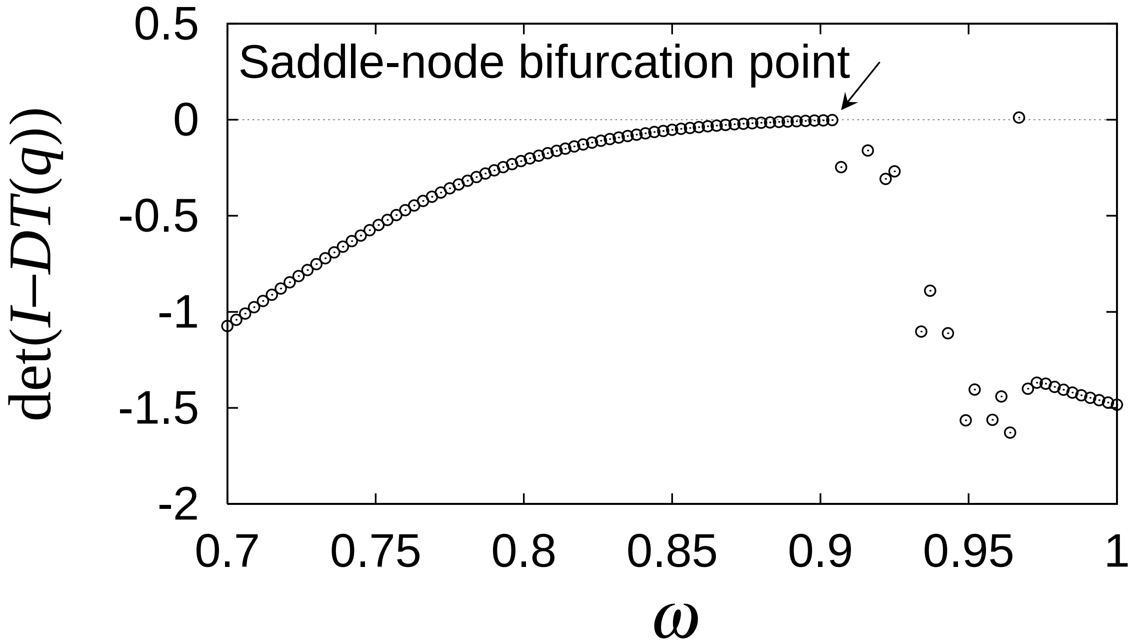


FIGURE 7. Characteristic polynomial $P(s) = |sI - DT(\boldsymbol{q})|$ for $s = 1$ as a function of a free parameter $\omega$. $P(1)$ vanishes at the saddle-node bifurcation point.

From the above result, we can suppose that the primary resonance (the large amplitude) in the response curve in Fig.3 undergoes a saddle-node bifurcation at $\omega \approx 0.91$ because the pair of the repeller and the 1-periodic attractor in Fig.4 for $\omega = 0.9$ vanishes in Fig.5 for $\omega = 0.95$ while the off resonance undergoes other types of bifurcation such as pitchfork bifurcations, Hopf bifurcations, and so on.

In what follows, we focus on the primary resonance undergoing the saddle-node bifurcation near $\omega = 0.91$ to investigate how it indicates the slow convergence of the synchronization errors.

3.2. **Numerical continuation of bifurcation points.** Let us summarize how to obtain bifurcation points numerically. See Refs[13, 14] for more details.

It is mathematically proved that a matrix representation $DT(\boldsymbol{q})$ of the linearization of the Poincaré map $T$ of the ordinary differential equation (12) is given by,

$$DT(\boldsymbol{q}) := J(\tau),\ \dot{J} = D\boldsymbol{f}(\boldsymbol{q}, t; \lambda)J,\ J(0) = I \tag{17}$$

where $D\boldsymbol{f}(\boldsymbol{q}, t; \lambda)$ is the Jacobian matrix and $I$ is the unit matrix. It can also be shown that the stabilities of the fixed point $\bar{\boldsymbol{q}}$ of the Poincaré map $T$ is characterized by the characteristic value $s$ satisfying the characteristic equation:

$$P(s) = |sI - DT(\bar{\boldsymbol{q}})| = 0. \tag{18}$$

From the basic theory of bifurcation[14], it is known that saddle-node bifurcations occurs at $s = 1$.

Figure 7 represents the value of characteristic polynomial for $s = 1$ calculated from Eqs (12) and (17) for $c = 0.04$. It is clearly seen that the value $P(1)$ vanishes near $\omega = 0.91$.

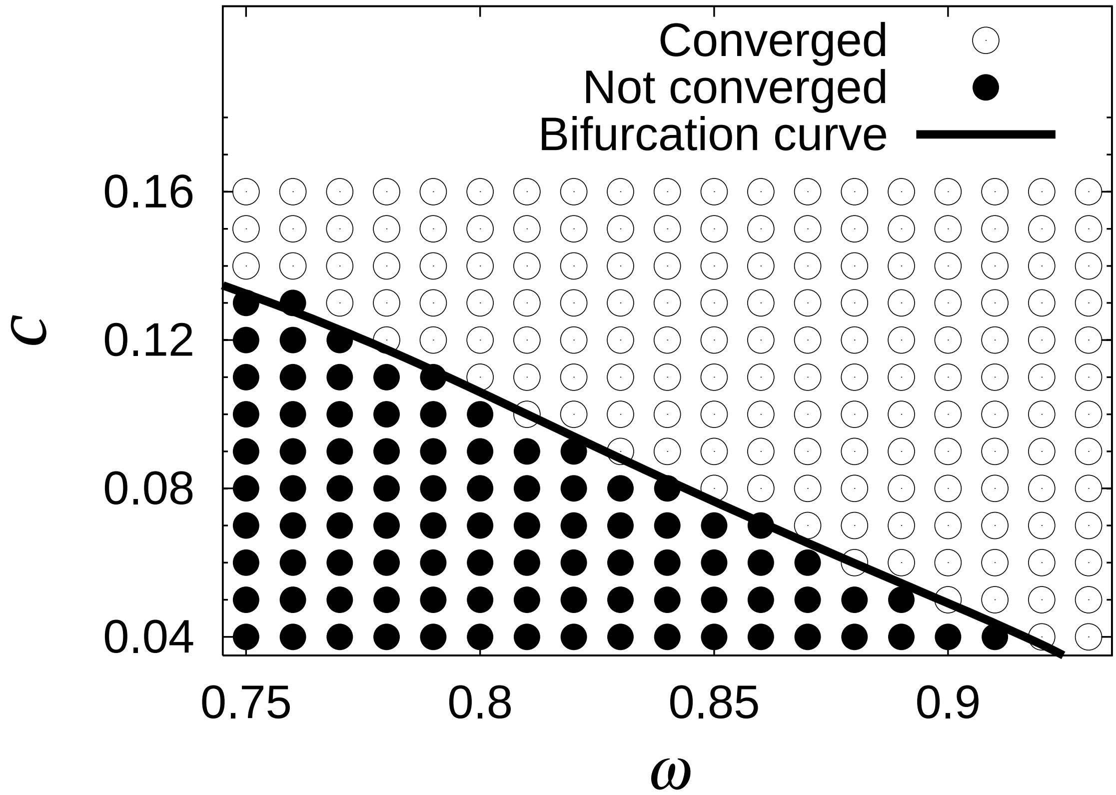


FIGURE 8. Numerical continuation of the saddle-node bifurcation point of periodic solutions of (8) and mean convergence time $\langle T \rangle$ of the synchronization errors. The white circles are plotted for $\langle T \rangle < 10^3$ and the black circles for otherwise respectively.

Since zeros of characteristic polynomials generally indicate bifurcation points[13], it is numerically proved that the primary resonance of the second moment undergoes the saddle-node bifurcation near $\omega = 0.91$.

3.3. **Saddle-node bifurcation sets indicating the slow convergence.** In order to continue the bifurcation points in the parameter space [14], we define new state vectors $\boldsymbol{p} := (\bar{\boldsymbol{q}}, \lambda) \in R^6$ and solve the equations (16) and (18) simultaneously:

$$T^m(\bar{\boldsymbol{q}}) = \bar{\boldsymbol{q}}, \quad P(s) = |sI - DT(\bar{\boldsymbol{q}})| = 0. \tag{19}$$

The solution $\boldsymbol{p}$ is called a bifurcation set of the map (16), and consequently yields a bifurcation set of the corresponding periodic solution of the MDE (8).

Figure 8 shows the saddle-node bifurcation set in the $(\omega, c)$-plane of periodic solutions of the MDE (8) and mean convergence time $\langle T \rangle$ of the synchronization errors. In practice, we consider the saddle-node bifurcation point in Fig.7 for $c = 0.04$ as the initial point and regard $\omega$ as the bifurcation parameter $\lambda$. We then solve the simultaneous equations (19) by standard Newton's methods. Shifting the second parameter as $c = 0.04 + j \cdot \Delta c$ ($j = 1, 2, \cdots$), we obtain a series of $\boldsymbol{p}$ on the $(\omega, c)$-plane where $\Delta c$ is a small value chosen for a good convergence of the Newton's methods.

The solid curve indicates the saddle-node bifurcation set of the MDE (8). The white and the black circles represent the fast $\langle T\rangle < 10^3$ and the slow $\langle T\rangle \geq 10^3$ convergences where $\langle T\rangle$ is calculated from Monte-Carlo simulations of the synchronization system (1). Along the bifurcation set, the solid curve, the characteristic polynomial takes zero values at which the stability changes. In other words, the changes of parameters crossing this curve transversely results in the stability change of the system.

It is very clear from the above result that the saddle-node bifurcation set belonging to the primary resonance indicated by the solid curve in Fig.8 is in good agreement with the threshold of occurrence of the slow convergence.

4. **Conclusions.** We have investigated how to characterize the slow convergence of the synchronization errors of the synchronization system which consists of the pair of the piecewise linear systems subjected to the common random excitation. We first have demonstrated numerically that the convergence speed of the synchronization errors significantly depends on the parameter conditions. It is shown that the slow convergence is caused by the multimodal probability densities so that it can be detected as the multi-valued solutions of the moment differential equations.

We then have constructed Poincaré maps of periodic solutions of the MDE to examine asymptotic behavior of the moments and clarify that the primary resonance encounters saddle-node bifurcations. We have numerically continued the bifurcation point to obtain the saddle-node bifurcation set of primary resonance of moments. It is clearly shown that the saddle-node bifurcation set belonging to the primary resonance is in good agreement with the threshold of occurrence of the slow convergence.

The above result leads to the conclusion that the saddle-node bifurcation set of the moment equations provides an effective identifier to detect the slow convergence of the synchronization errors.

## REFERENCES


[1] R. Toral, C.R. Mirasso, E. Hernández-García, and O. Piro, Analytical and numerical studies of noise-induced synchronization of chaotic systems, *Chaos*, vol.11, no.3, pp.665-673, 2001.

[2] H. Suetani, T. Horita, and S. Mizutani, Noise-induced enhancement of fluctuation and spurious synchronization in uncoupled type-I intermittent chaotic systems, *Phys. Rev. E*, vol.69, pp.016219, 2004.

[3] A. Stefański and T. Kapitaniak, Synchronization of mechanical systems driven by chaotic or random excitation, *J. Sound and Vibration*, vol.260, pp.565-576, 2003.

[4] C.S. Zhou, J. Kurths, E. Allaria, S. Boccaletti, R. Meucci, and F.T. Arecchi, Constructive effects of noise in homoclinic chaotic systems, *Phys. Rev. E*, vol.67, pp.066220, 2003.

[5] A.B. Neiman and D.F. Russell, Synchronization of noise-induced bursts in noncoupled sensory neurons, *Phys. Rev. Lett.*, vol.88, no.13, pp.138103, 2002.

[6] K. Yoshida and K. Sato, Noise-induced synchronization without coupling, *Trans. JSME Series C (in Japanese)*, vol.70, no.696, pp.2228-2234, 2004.

[7] K. Yoshida, K. Sato, and A. Sugamaga, Noise-induced synchronization of uncoupled nonlinear systems, *J. Sound and Vibration*, vol.290, pp.34-47, 2006.

[8] K. Yoshida and Y. Nishizawa, Convergence property of noise-induced synchronization, *Proccedings of the 38rd ISCIE International Symposium on Stochastic Systems Theory and its Applications, November 9-10, 2006, Suwa, Japan*, pp.7-12, 2007.

[9] K. Yoshida and Y. Nishizawa, Convergence property of noise-induced synchronization, *Int. J Innovative Computing, Information and Control*, vol.4, no.1, pp.79-89, 2008.

[10] Y.K. Lin and G.Q. Cai, *Probabilistic Structural Dynamics*, McGraw-Hill, pp.281-304, 1979.

[11] S. Keijin, K. Osamu, Y. Sumio, and T. Nobuo, Jump phenomena in gear system to random excitation, *Trans. JSME series C (in Japanese)*, vol.50, no.458, pp.1849-1856, 1984.

[12] B. Øksendal, *Stochastic Differential Equation*, Springer-Verlag, Berlin, 1998.

[13] J. Guckenheimer and P. Holmes, *Nonlinear Oscillations, Dynamical Systems, and Bifurcations of Vector Fields*, Springer-Verlag, New York, pp.22-32, 1983.

[14] H. Kawakami, Bifurcation of periodic responses in forced dynamic nonlinear circuits: Computation of bifurcation values of the system parameters, *Trans. IEEE CAS*, vol.31, no.3, pp.248-260, 1984.